J. Fluid Mech. (1997), *vol.* 353, *pp.* 45–66. Printed in the United Kingdom

© 1997 Cambridge University Press

On the stability of vertical double-diffusive interfaces. Part 3. Cylindrical interface

By I. A. ELTAYEB[1] AND D. E. LOPER[2]

[1] Department of Mathematics and Statistics, Sultan Qaboos University, Muscat, Sultanate of Oman

[2] Geophysical Fluid Dynamics Institute, Florida State University, Tallahassee, FL 32306-3017, USA

(Received 10 September 1996 and in revised form 8 May 1997)

This is the final part of a three-part study of the stability of vertically oriented double-diffusive interfaces having an imposed vertical stable temperature gradient. In this study, flow is forced within a fluid of infinite extent by a prescribed excess of compositionally buoyant material within a circular cylindrical interface. Compositional diffusivity is ignored while thermal diffusivity and viscosity are finite. The instability of the interface is determined by quantifying the exponential growth rate of a harmonic deflection of infinitesimal amplitude. Attention is focused on the zonal wavenumber of the fastest growing mode.

The interface is found to be unstable for some wavenumber for all values of the Prandtl number and interface radius. The zonal wavenumber of the fastest growing mode increases roughly linearly with interface radius, except for small values of the Prandtl number (< 0.065). For small and moderate values of the radius, the preferred mode is either axisymmetric or has zonal wavenumber of 1, representing a helical instability. The growth rate of the fastest-growing mode is largest for interfaces having radii of from 2 to 3 salt-finger lengths.

1. Introduction

This is the final part of a three-part study of vertically oriented double-diffusive interfaces. The first part (Eltayeb & Loper 1991, hereinafter referred to as Part 1) focused on the stability of a single plane interface, consisting of a sharp discontinuity of composition and hence buoyancy, in an infinite extent of fluid having a stabilizing thermal gradient. The fluid was subject to the combined action of thermal diffusivity and viscosity, but compositional diffusivity was assumed negligibly small. It was found that a small-amplitude harmonic distortion of the interface grows exponentially with time for all values of the Prandtl number $\sigma(=\nu/\kappa$, where ν is the viscosity and κ is the thermal diffusivity). The fastest-growing mode has variation only in the vertical direction for $\sigma < 0.065$, but is oblique to the vertical for $\sigma > 0.065$. The second part (Eltayeb & Loper 1994, hereinafter referred to as Part 2) investigated the stability of two parallel interfaces having equal and opposite compositional jumps, forming a slab of buoyant material. This configuration will be referred to as the Cartesian plume in what follows. Solutions to this problem can take one of two uncoupled forms: a sinuous mode in which the small-amplitude harmonic distortions of the two interfaces are in phase and a varicose mode having the distortions out of phase. Instability again occurs for all values of the Prandtl number, with the fastest-growing mode of instability being either sinuous oblique, varicose oblique, sinuous vertical or varicose

https://doi.org/10.1017/S0022112097007374 Published online by Cambridge University Press

vertical depending on the prescribed values of Prandtl number and interfacial separation distance.

In this third part of the study we examine the stability of a circular cylindrical interface. The present problem is more physically interesting than those studied in Part 1 and Part 2, as it represents more closely the fresh-water plumes in an aqueous ammonium-chloride solution exhibited in figure 1 of Part 1 (see also Chen & Chen 1991; Hellawell, Sarazin & Steube 1993; Chen 1995; Worster 1997), as well as plumes which arise in other situations. Most previous work on directional solidification deals with the flows and stability of the mushy layer that develops between the solid and fluid (see e.g. Chen 1995 and Worster 1997, and references therein). The stability of the buoyant plumes that emanate from the mushy layer have not attracted much attention. Hellawell *et al.* (1993) have performed an experimental study of the flow and development of plumes in aqueous, metallic and organic alloys. They found that plumes are, to a good approximation, in the form of vertical cylinders originating in the permeable dendritic structure of the mushy layer. Their radii are fairly uniform, but show a slight increase with height. As the solidification front rises, the plumes develop instabilities at the top where they break-up and spread horizontally. In the case of aqueous solutions these events take place rapidly but the time scale for organic solutions is longer and provides better opportunities for observation.

This study was initially motivated by a desire to understand small-scale motions in Earth's core which are driven by compositional buoyancy generated during the solidification of the inner core and are possibly associated with the dynamo process which maintains Earth's magnetic field (e.g. see Loper & Moffatt 1993; Moffatt & Loper 1994). However, the results may be applicable to problems which arise in metallurgy during the solidification of metallic alloys (Copley *et al.* 1970), in the evolution of magma chambers (Jaupart & Tait 1995) and in the solidification of sea water (Wettlauffer, Worster & Huppert 1996).

Of particular physical interest is identification of the circumstances in which the instability having a zonal wavenumber of 1 may occur. This mode is preferred for the cylindrical interfaces produced in the ammonium-chloride experiments. It should be noted that this mode, in which the plume axis assumes a helical shape, has no clear counterpart on the planar interfaces studied in Parts 1 and 2.

In what follows, we consider the stability of a vertical circular interface of radius s_0 surrounding compositionally buoyant fluid immersed in an infinite fluid which is compositionally less buoyant. The temperature increases uniformly with height, giving the fluid a uniform stable density profile; see figure 1. This configuration, which we shall refer to as the cylindrical plume, is very similar to that studied by Howard & Veronis (1987, 1992); we are in effect considering their configuration but with a single isolated plume of circular cross-section. As in their model and in Parts 1 and 2, material diffusion is assumed negligibly small, while viscosity and thermal diffusion are included. The conditions under which this assumption is valid are discussed in § 5.4 of Part 1.

The density, ρ, of the fluid is assumed to depend on the temperature, T, and the concentration, C, of buoyant material through the linear relationship

$$\rho/\rho_0 = 1-\alpha(T-T_0)-\beta(C-C_0), \tag{1.1}$$

where α is the coefficient of thermal expansion, β is the coefficient of compositional expansion and a subscript 0 denotes a constant reference value. The composition of the ambient fluid is equal to C_0 while that within the interface is $C_0+\tilde{C}$. In what follows, we shall assume that α, β and $\tilde{C}$ are constant and positive. In the absence of thermal

https://doi.org/10.1017/S0022112097007374 Published online by Cambridge University Press

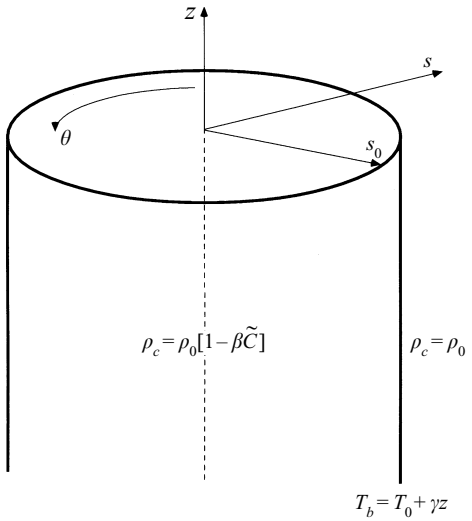


FIGURE 1. A schematic representation of the physical configuration of the compositionally buoyant plume. ρ_c denotes the density with thermal effects ignored and T_b denotes the background temperature. The vertical temperature gradient is represented by γ.

diffusion, the jump in density across the interface would be compensated by an opposite jump in temperature, making the density continuous and, in fact, uniform. However, thermal diffusion across the interface smooths out the temperature jump, creating a baroclinic density profile which drives vertical flow. The solutions for the radial variation of temperature and vertical flow adjacent to the interface are expressed in terms of Kelvin functions by formulas (1:3.20) and (1:3.21).†

The possible perturbations of the circular interface fall into three categories depending on the value of the zonal wavenumber, q. For $q = 0$, the perturbation is axisymmetric, representing a (local) change in size of the interface with no change of shape. For $q = 1$, the interface is displaced laterally without change of size or shape. If the direction of displacement varies in the vertical direction, the shape of the interface is helical. For $q \geqslant 2$, the interface experiences a change of shape but not size. It is clear from figure 1:1 that the helical mode $q = 1$ is preferred for a solution of ammonium chloride and water. The helical mode appears to be preferred for a solution of isopropanol and water (M. G. Worster, private communication), while the axisymmetric mode $q = 0$ is seen by Wettlauffer *et al.* (1996) in their study of sodium chloride and water. A primary goal of the analysis of this paper is to predict the zonal wavenumber of the fastest-growing mode as a function of the Prandtl number and the interface radius.

The formulation of the present problem, given in §2, follows closely that of Part 1 and Part 2, but the solution procedure employed here differs. As in Parts 1 and 2, the flow variables are divided into three parts, consisting of a static background state, a basic state associated with thermal diffusion across the undeformed interface and a perturbation of infinitesimal amplitude associated with the harmonic deflection of the interface (see (2.24) below). The forcing for the perturbed variables is measured by the Reynolds number, R, which is proportional to the magnitude of the compositionally

† In what follows, equation $(x.y)$ of Part 1 will be referred to as $(1{:}x.y)$, figure z of Part 1 will be referred to as figure $1{:}z$ and section $x.y$ will be referred to as §$1{:}x.y$.

https://doi.org/10.1017/S0022112097007374 Published online by Cambridge University Press

induced density jump across the interface (see (2.5) and (2.6) below). Since the basic state is baroclinic, there is no minimum critical Reynolds number; the flow is unstable for any non-zero value of R. The amplitude of the perturbation variables, as well as the temporal growth rate, are expanded in powers of R. It is anticipated that the most unstable mode occurring for small values of R provides a 'template' for the nonlinear mode which is actually observed; this assumption is the essence of Landau's theory of nonlinear stability (e.g. see Drazin & Reid 1981, p. 370). If this assumption is correct for the problem at hand, then the most unstable modes found herein should correlate with the modes observed in the ammonium-chloride experiments, as well as in other physical situations. In Part 2 it was found that to leading order, the growth rate was proportional to R and imaginary, indicating a neutral oscillation. This neutral oscillation is the obvious consequence of the requirement that the basic flow and temperature confirm kinematically to the deformed interface. The real part of the growth rate was found to be of order R^2. The same situation occurs in the present problem.

In Parts 1 and 2 the stability was determined by systematically solving analytically the leading-order and first-order problems in powers of R for both flow variables and growth rate. This procedure is straightforward, though somewhat tedious in the case of two parallel interfaces. In the case of a cylindrical plume, this procedure cannot be completed analytically because closed-form solutions of the non-homogeneous equations for the first-order variables are not known. Rather than resorting to numerical solution of the problem, an alternative analytic procedure is employed in §3. In this procedure we abandon the attempt to find the perturbation variables to first order, and concentrate on obtaining an expression for the real part of the growth rate which contains only basic-state and leading-order perturbation variables. Since this is a challenging and somewhat novel procedure, the analysis is presented in some detail in an Appendix.

The result of the analysis of §3 is an expression for the growth rate of the disturbance as a function of Prandtl number (σ), interface radius (s_0) and the zonal (q) and vertical (n) wavenumbers describing the harmonic perturbation. The expression is an integral over radial distance, from the axis to infinity, which must be evaluated numerically. The results of this evaluation are presented in §4. Specifically, the growth rate is maximized over the two 'internal' variables q and n. Of particular interest is the value of q associated with the maximum growth rate, as a function of σ and s_0. These values are presented on the 'regime diagram' in figure 4, and the special nature of the axisymmetric and helical modes (having $q = 0$ and 1) is elucidated. Finally in §5 the solution procedure and results are summarized, some comments are made regarding the physical mechanism of instability and the limitations of the present model are discussed.

2. Formulation

We consider the stability of the axisymmetric flow due to a vertical column of compositionally buoyant liquid immersed within a stably stratified liquid. The buoyant column is assumed to be circularly cylindrical, composition within it is assumed uniform and diffusion of material is neglected. The aim of the analysis is to develop an expression for the stability of this column when subject to harmonic perturbations of infinitesimal amplitude.

For brevity, we shall present the governing equations only in dimensionless form; for dimensional versions, the reader may refer to Part 1. The relevant equations are

https://doi.org/10.1017/S0022112097007374 Published online by Cambridge University Press

$$\partial \boldsymbol{u}/\partial t + R\boldsymbol{u}\cdot\boldsymbol{\nabla}\boldsymbol{u} = -\boldsymbol{\nabla}p + \nabla^2\boldsymbol{u} + \rho/\rho_0\,\hat{\boldsymbol{z}}, \tag{2.1}$$

$$\boldsymbol{\nabla}\cdot\boldsymbol{u} = 0, \tag{2.2}$$

$$\sigma(\partial T/\partial t + R\boldsymbol{u}\cdot\boldsymbol{\nabla}T) + \boldsymbol{u}\cdot\hat{\boldsymbol{z}} = \nabla^2 T, \tag{2.3}$$

$$\partial C/\partial t + R\boldsymbol{u}\cdot\boldsymbol{\nabla}C = 0, \tag{2.4}$$

plus (1.1). Here $\boldsymbol{u}$ is the fluid velocity vector and p is the pressure, and we have defined the Prandtl and Reynolds numbers, respectively, by

$$\sigma = \nu/\kappa, \quad R = UL/\nu \tag{2.5}$$

where ν is the kinematic viscosity, κ is the thermal diffusivity and L, U are units of length and velocity associated with salt fingers, defined by

$$L = (\nu\kappa/\alpha\gamma g)^{1/4}, \quad U = \beta\tilde{C}(g\kappa/\alpha\gamma\nu)^{1/2}. \tag{2.6}$$

In these equations g is the acceleration due to gravity, γ is the uniform vertical temperature gradient and $\beta\tilde{C}$ is the magnitude of the relative density deficit $\Delta\rho/\rho_0$ of the buoyant fluid. The temperature is scaled with $\beta\tilde{C}/\alpha$, the composition with $\tilde{C}$ and the pressure with $\rho_0\beta\tilde{C}(g^3\nu\kappa/\alpha\gamma)^{1/4}$.

We shall assume that the variables consist of a static background state denoted by a subscript b, a basic state (driven by lateral diffusion of heat) denoted by an overbar and a perturbation, denoted by a dagger:

$$\boldsymbol{u} = \bar{\omega}\hat{\boldsymbol{z}} + \epsilon\boldsymbol{u}^\dagger, \qquad C = C_b + \bar{C} + \epsilon C^\dagger, \tag{2.7a, b}$$

$$T = T_b + \bar{T} + \epsilon T^\dagger, \qquad p = p_b + \bar{p} + \epsilon p^\dagger, \tag{2.7c, d}$$

where C_b is a constant,

$$T_b = T_0 + (z - z_0)/\sigma R, \tag{2.8}$$

and

$$p_b = p_0 - (z - z_0)/\beta\tilde{C} + (z - z_0)^2/2\sigma R. \tag{2.9}$$

The basic-state solutions associated with the cylindrical interface are given by (1:3.17), (1:3.20) and (1:3.21). Using formulas (9.9.1), (9.9.2), (9.9.16) and (9.9.17) of Abramowitz & Stegun (1970), these may be expressed as

$$\bar{C}(s; s_0) = 1 - H(s - s_0), \quad \bar{p}(s; s_0) = 0, \tag{2.10a, b}$$

$$\bar{w}(s; s_0) = \mathrm{Im}[\tilde{w}], \quad \bar{T}(s; s_0) = \mathrm{Im}[\tilde{T}], \tag{2.10c, d}$$

where

$$\tilde{w} = \begin{cases} ks_0 K'(ks_0) I(ks) & \text{for} \quad s < s_0 \\ ks_0 I'(ks_0) K(ks) & \text{for} \quad s_0 < s, \end{cases} \tag{2.11}$$

$$\tilde{T} = \begin{cases} -\mathrm{i}ks_0 K'(ks_0) I(ks) - i & \text{for} \quad s < s_0 \\ -\mathrm{i}ks_0 I'(ks_0) K(ks) & \text{for} \quad s_0 < s, \end{cases} \tag{2.12}$$

$$k = \exp(\mathrm{i}\pi/4) = (1 + \mathrm{i})/\sqrt{2}. \tag{2.13}$$

Here H is the Heaviside step function, s is a cylindrical radial coordinate, s_0 is a free parameter representing the (dimensionless) radius of the cylindrical plume, a prime denotes differentiation and I and K are modified Bessel functions (of complex argument).

The perturbations satisfy the homogeneous equations (1:2.16)–(1:2.18), i.e.

$$\boldsymbol{\nabla}\cdot\boldsymbol{u}^\dagger = 0, \tag{2.14}$$

$$\partial \boldsymbol{u}^\dagger/\partial t + R[\bar{w}(\partial \boldsymbol{u}^\dagger/\partial z) + (\boldsymbol{u}^\dagger\cdot\boldsymbol{\nabla}\bar{w})\,\hat{\boldsymbol{z}}] = -\boldsymbol{\nabla}p\dagger + \nabla^2\boldsymbol{u}^\dagger + (T^\dagger + C^\dagger)\,\hat{\boldsymbol{z}}, \tag{2.15}$$

$$\sigma\partial T^\dagger/\partial t + \sigma R[\bar{w}(\partial T^\dagger/\partial z) + \boldsymbol{u}^\dagger\cdot\boldsymbol{\nabla}\bar{T}] + \boldsymbol{u}^\dagger\cdot\hat{\boldsymbol{z}} = \nabla^2 T^\dagger, \tag{2.16}$$

$$\partial C^\dagger/\partial t + R[\bar{w}(\partial C^\dagger/\partial z) + \boldsymbol{u}^\dagger\cdot\boldsymbol{\nabla}\bar{C}] = 0. \tag{2.17}$$

https://doi.org/10.1017/S0022112097007374 Published online by Cambridge University Press

Note that the divergence of (2.15) gives

$$\boldsymbol{\nabla}^2 p^\dagger = \partial(T^\dagger - 2\boldsymbol{R}\boldsymbol{u}^\dagger \cdot \boldsymbol{\nabla}\bar{w})/\partial z. \tag{2.18}$$

Equation (2.17) states that the composition of a parcel is preserved, as material diffusion has been ignored. Consequently after radial deflection of the interface by a small amount, η, the composition is given by

$$\bar{C} + \epsilon C^\dagger = 1 - H(s - s_0 - \eta). \tag{2.19}$$

Combining this with (2.10a), we obtain

$$C^\dagger = \frac{H(s-s_0) - H(s-s_0-\eta)}{\epsilon}. \tag{2.20}$$

Since $\eta = O(\epsilon)$, we see that $C^\dagger$ behaves essentially as a delta-function forcing for the problem, having a very large amplitude over a narrow radial range near $s = s_0$. Outside this narrow range, $C^\dagger$ is equal to zero. If we were to use (2.20) as a forcing for the problem, the perturbation solution would not be uniformly valid. However, due to the large values of viscosity and thermal diffusivity compared with material diffusivity, the temperature and flow variables respond only to the integrated effect of (2.20). Howard & Veronis (1992) encountered a similar non-uniformity in their analysis of an array of salt fingers, and got around the difficulty by using a smoothed salinity profile. We adopt an alternative procedure, using (2.20) to develop a boundary condition on the perturbation variables which permits a solution which is uniformly valid in s. This is accomplished as follows. After subtracting the static and basic-state solutions, the vertical component of the momentum equation becomes

$$\frac{\partial^2 w^\dagger}{\partial s^2} = F^\dagger - C^\dagger \tag{2.21}$$

where

$$F^\dagger = -\frac{1}{s}\frac{\partial w^\dagger}{\partial s} - \frac{1}{s^2}\frac{\partial^2 w^\dagger}{\partial \theta^2} - \frac{\partial^2 w^\dagger}{\partial z^2} + \frac{\partial w^\dagger}{\partial t} + R\bar{w}\frac{\partial w^\dagger}{\partial z} + R(\boldsymbol{u}^\dagger \cdot \boldsymbol{\nabla})(\bar{w} + \epsilon\omega^\dagger) + \frac{\partial p^\dagger}{\partial z} - T^\dagger. \tag{2.22}$$

Let us integrate (2.21) from $s = s_0 - \delta$ to $s = s_0 + \eta + \delta$, where δ is a radial distance much smaller than ϵ. (We have assumed that $\eta > 0$ for definiteness; the result is valid for $\eta < 0$ as well.) Within this small interval, $F^\dagger$ is of unit order, while $C^\dagger$ is large, equal to $1/\epsilon$. Consequently we have

$$\left\langle \frac{\partial w^\dagger}{\partial s} \right\rangle = -\frac{\eta}{\epsilon} + O(\eta), \tag{2.23}$$

where $\langle f \rangle = f(s_0 + \eta +) - f(s_0 -)$. Equation (2.23) is a non-homogeneous boundary condition which supplies the forcing for the problem. With $\eta = O(\epsilon)$, the forcing in (2.23) is of unit order, allowing the solution to be uniformly valid in s. In what follows we shall set $C^\dagger$ equal to zero and employ condition (2.23).

If we introduce a cylindrical coordinate system s, θ, z and write

$$\left.\begin{aligned} \{\boldsymbol{u}\dagger, p^\dagger, T^\dagger\} &= \{\mathrm{i}u, v, w, \mathrm{i}np, T\}\exp[\mathrm{i}(q\theta + nz) + \Omega t] + \text{c.c.} \\ \eta &= \epsilon \exp[\mathrm{i}(q\theta + nz) + \Omega t] + \text{c.c.}, \end{aligned}\right\} \tag{2.24}$$

and the equations governing the perturbation variables maybe expressed in component form as

$$\mathrm{d}(su)/\mathrm{d}s + qv + nsw = 0, \tag{2.25}$$

$$s^2 \mathrm{L}(v) - v - \bar{\Omega} s^2 v = -qnsp + 2qu, \tag{2.26}$$

$$\mathrm{L}(w) - \bar{\Omega} w = \mathrm{i}R(\mathrm{d}\bar{w}/\mathrm{d}s)\, u - n^2 p - T, \tag{2.27}$$

$$\mathrm{L}(T) - \sigma\bar{\Omega} T = w + \mathrm{i}\sigma R(\mathrm{d}\bar{T}/\mathrm{d}s)\, u, \tag{2.28}$$

https://doi.org/10.1017/S0022112097007374 Published online by Cambridge University Press

and

$$\mathrm{L}(p) = T - 2\mathrm{i}R(\mathrm{d}\bar{w}/\mathrm{d}s)\,u, \tag{2.29}$$

where

$$\mathrm{L} = \frac{\mathrm{d}^2}{\mathrm{d}s^2} + \frac{\mathrm{d}}{s\,\mathrm{d}s} - \frac{q^2}{s^2} - n^2 \tag{2.30}$$

and

$$\bar{\Omega} = \Omega + \mathrm{i}nR\bar{w}. \tag{2.31}$$

The set of equations (2.25)–(2.29) is to be solved subject to the following conditions:

at $s = 0$ the perturbation functions are analytic; (2.32)

at $s = s_0$ u, v, w, p, T, $\mathrm{d}v/\mathrm{d}s$ and $\mathrm{d}t/\mathrm{d}s$ are continuous, (2.33)

$$\langle \mathrm{d}w/\mathrm{d}s \rangle = -1, \tag{2.34}$$

$$\langle \mathrm{d}p/\mathrm{d}s \rangle = 1 \tag{2.35}$$

and

$$Ru = -\mathrm{i}\bar{\Omega}; \tag{2.36}$$

as $s \to \infty$ the perturbation functions decay to zero. (2.37)

where now

$$\langle z \rangle = z(s_0+) - z(s_0-). \tag{2.38}$$

Condition (2.34) is the normalized version of (2.23) and condition (2.35) may be verified by combining the s-derivative of (2.25) with the radial component of (2.15) and the remaining conditions.

Here Ω is the growth rate of the perturbation; if $\mathrm{Re}(\Omega) > 0$, instability occurs. Note that $\bar{w}$, $\bar{T}$, and $\bar{\Omega}$ are functions of s. The problem becomes equivalent to that studied in Part 1 in the limit $s_0 \to \infty$. Specifically if we let $s = s_0 + x$, $q = s_0 m$, and take the limit $s_0 \to \infty$, equations (2.25)–(2.29) reduce to (1:4.3), (1:4.5)–(1:4.7) and (1:4.13).

The problem stated by (2.25)–(2.37) has symmetry properties similar to those of the Cartesian plume studied in Part 2. The basic-state functions $\bar{w}$ and $\bar{T}$ are even functions of s and their derivatives are odd, and the operator L preserves symmetry. It follows that the problem has solutions of even parity, in which w, p and T are even in s and u and v are odd, and odd parity, in which w, p and T are odd in s and u and v are even. Note the difference in the symmetry of the horizontal velocity component parallel to the interface, v, in the cylindrical plume from that for the Cartesian plume. These symmetries are of use in simplifying the problem of the Cartesian plume because deflections of the two interfaces are decoupled in that problem. Since the cylindrical problem involves a single interface, these symmetry properties do not lead to any simplification.

It should also be noted that the axisymmetric case, having $q = 0$, behaves differently from the non-axisymmetric cases, having $q > 1$. In the axisymmetric case, the perturbation functions can have non-zero values at $s = 0$, whereas in the non-axisymmetric case, single-valuedness requires that perturbations be zero at the axis.

We are interested in finding the behaviour of the system in the limit of small R. In this case it is natural to write

$$\{u, v, w, p, T\} = \sum_{\alpha=0}^{\infty} \{u_\alpha, v_\alpha, w_\alpha, p_\alpha, T_\alpha\}\, R^\alpha, \quad \Omega = \sum_{\alpha=1}^{\infty} \Omega_\alpha R^\alpha. \tag{2.39}$$

Upon substitution of this ansatz into the governing equations, we obtain a sequence

https://doi.org/10.1017/S0022112097007374 Published online by Cambridge University Press

of problems, ordered in powers of R. Stability of the plume is determined by the first of the sequence Ω_α which has a non-zero real part. As it happens, Ω_1 is imaginary, and we need to determine Ω_2. Expression for Ω_1 and Ω_2 are presented in the next section.

3. Solution of the stability problem

In this section we summarize the solutions of the sets of equations corresponding to the first two terms in the expansions (2.39). We shall refer to the leading-order set of equations and boundary conditions as Problem 0 and the first-order set as Problem 1.

3.1. *Problem 0*

Upon substitution of (2.39) into (2.25)–(2.29), the dominant-order equations are obtained:

$$\mathrm{d}(su_0)/\mathrm{d}s + qv_0 = -nsw_0, \tag{3.1}$$

$$s^2\mathrm{L}(v_0) - v_0 - 2qu_0 = -qnsp_0, \tag{3.2}$$

$$\mathrm{L}(w_0) + n^2p_0 + T_0 = 0, \tag{3.3}$$

$$\mathrm{L}(T_0) - w_0 = 0 \tag{3.4}$$

and

$$\mathrm{L}(p_0) - T_0 = 0. \tag{3.5}$$

These equations are to be solved subject to the boundary conditions obtained from (2.32)–(2.35) and (2.37) by attaching a subscript 0 to all the relevant variables; using (2.31) condition (2.36) becomes

$$\text{at } s = s_0 \qquad u_0 = -\mathrm{i}\Omega_1 + n\bar{w}. \tag{3.6}$$

The solutions may be expressed as

$$\{w_0, p_0, T_0\} = s_0 \sum_{j=1}^{3} \{\mu_j^3, \mu_j, \mu_j^2\} B_j R_j, \tag{3.7}$$

$$u_0 = ns_0 \sum_{j=1}^{3} B_j \xi_j \begin{cases} K_q(\xi_j s_0) I_q'(\xi_j s) & \text{for} \quad 0 < s < s_0 \\ I_q(\xi_j s_0) K_q'(\xi_j s) & \text{for} \quad s_0 < s, \end{cases} \tag{3.8}$$

$$v_0 = -\frac{nqs_0}{s} \sum_{j=1}^{3} B_j R_j, \tag{3.9}$$

where

$$R_j = \begin{cases} K_q(\xi_j s_0) I_q(\xi_j s) & \text{for} \quad 0 < s < s_0 \\ I_q(\xi_j s_0) K_q(\xi_j s) & \text{for} \quad s_0 < s, \end{cases} \tag{3.10}$$

$$B_j = \frac{\mu_j^2}{3n^2 + 2\mu_j}, \tag{3.11}$$

$$\xi_j^2 = \mu_j + n^2, \tag{3.12}$$

and μ_j are solutions of

$$\mu^3 + \mu + n^2 = 0. \tag{3.13}$$

The growth rate of the perturbation to dominant order may be determined from (3.6). Using (2.11) and (3.8) we have

$$\Omega_1 = \mathrm{i}ns_0 \left\{ \sum_{j=1}^{3} K_j \xi_j I_q'(\xi_j s_0) I_q(\xi_j s_0) - \mathrm{Im}\left[kI'(ks_0) K(ks_0)\right] \right\}. \tag{3.14}$$

https://doi.org/10.1017/S0022112097007374 Published online by Cambridge University Press

The expression in the curly brackets is real and consequently Ω_1 is imaginary. We will see later that Ω_2 is real so that the phase speeds in the vertical and zonal directions, U_z, U_θ, respectively, correct to order R^2, are given by

$$U_z = \mathrm{i}\Omega_1/n, \quad U_\theta = \mathrm{i}\Omega_1 s_0/q. \tag{3.15}$$

These functions are plotted in figures 2 and 3 are discussed in §4.

3.2. *Problem 1*

We now consider the first-order set of equations and boundary conditions in order to determine the growth rate Ω_2. Previously, for the problems of the single plane interface and two parallel interfaces, this was accomplished by solving the first-order problem in full. This is a formidable analytical task in the Cartesian cases, and appears to be insurmountable in the cylindrical case, suggesting that a numerical solution is in order. However, it is possible to find Ω_2 by means of a compatibility or solvability integral which involves only zeroth-order quantities, thereby circumventing the need to solve the full first-order problem. This procedure is similar to that leading to a standard solvability condition for a perturbed eigenvalue problem, except that the analysis is considerably more complicated in the present case. This process, which is presented in the Appendix, has been employed to re-solve the problems of the single plane interface and two parallel interfaces and has yielded identical results of those in Part 1 and Part 2. Copies of these calculations are available from either author on request.

The solvability integral is

$$\Omega_2 = \int_0^\infty \left[\frac{\mathrm{d}\bar{w}}{\mathrm{d}s}\left(\frac{q^2 R_n}{s} - \frac{\mathrm{d}H_n}{\mathrm{d}s}\right) - n(\mathrm{i}\Omega_1 - n\bar{w})\, H_n\right] \sum_{j=1}^{3} \frac{\mu_j^2 R_j}{3n^2 + 2\mu_j}\, s\, \mathrm{d}s$$
$$- \frac{\mathrm{i}}{n}\int_0^\infty \left\{[F_p + F_w]\, H_n - \sum_{j=1}^{3} [(1+\mu_j^2) F_p + F_w + \mu_j F_T] \frac{n^2 H_j}{3n^2 + 2\mu_j}\right\} \frac{s}{s_0}\, \mathrm{d}s, \tag{3.16}$$

where

$$F_p = -2\mathrm{i}(\mathrm{d}\bar{w}/\mathrm{d}s)\, u_0, \tag{3.17}$$

$$F_w = \mathrm{i}(\mathrm{d}\bar{w}/\mathrm{d}s)\, u_0 + (\Omega_1 + \mathrm{i}n\bar{w})\, w_0, \tag{3.18}$$

$$F_T = \mathrm{i}\sigma(\mathrm{d}\bar{T}/\mathrm{d}s)\, u_0 + \sigma(\Omega_1 + \mathrm{i}n\bar{w})\, T_0, \tag{3.19}$$

$$H_n(s; s_0) = n s_0 \begin{cases} K_q'(n s_0)\, I_q(ns) & \text{for} \quad 0 < s < s_0 \\ I_q'(n s_0)\, K_q(ns) & \text{for} \quad s_0 < s, \end{cases} \tag{3.20}$$

$$R_n(s; s_0) = \begin{cases} K_q(n s_0)\, I_q(ns) & \text{for} \quad 0 < s < s_0 \\ I_q(n s_0)\, K_q(ns) & \text{for} \quad s_0 < s \end{cases} \tag{3.21}$$

and

$$H_j(s; s_0) = \xi_j s_0 \begin{cases} K_q'(\xi_j s_0)\, I_q(\xi_j s) & \text{for} \quad 0 < s < s_0 \\ I_q'(\xi_j s_0)\, K_q(\xi_j s) & \text{for} \quad s_0 < s. \end{cases} \tag{3.22}$$

Ω_1 is given by (3.14), μ_j are solutions of (3.13), the leading-order variables are given by (3.7)–(3.9) and the basic-state variables by (2.10)–(2.12). Formula (3.16) is the desired representation of Ω_2 in terms of integrals of leading-order and basic-state quantities, which is quantified and discussed in the next section.

4. Evaluation and discussion of growth rates

The cylindrical interface is unstable to a harmonic perturbation of infinitesimal amplitude if the real part of Ω is positive. Ω is a function of the zonal and vertical wavenumbers, q and n, which are internal variables, and three external variables: the

https://doi.org/10.1017/S0022112097007374 Published online by Cambridge University Press

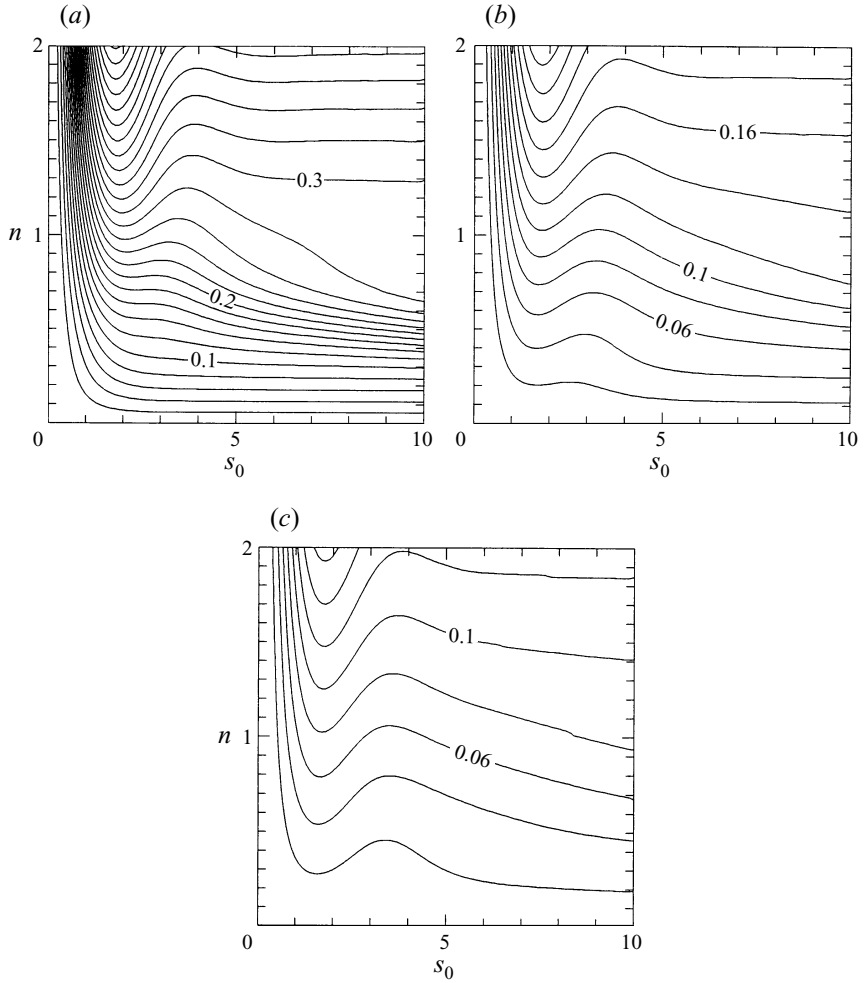


FIGURE 2. Isoline plots of the zonal phase speed, U_θ, on the (s_0, n)-plane for (*a*) $q = 1$, (*b*) 2 and (*c*) 3. The contour interval is 0.02.

Prandtl number σ, the interface radius s_0 and the Reynolds number R. Since the basic state is baroclinic, there is no minimum critical value of R; the stability analysis has been simplified by expanding Ω in a Taylor series in powers of R. Due to the scaling adopted, there is no zeroth-order term and the series begins like

$$\Omega(s_0, \sigma, R; q, n) = \Omega_1(s_0; q, n)\, R + \Omega_2(s_0, \sigma; q, n)\, R^2 + \ldots. \tag{4.1}$$

We found in §3, as in Parts 1 and 2, that Ω_1 is imaginary and Ω_2 is real. The result that Ω_1 is imaginary is expected on physical grounds; this and the associated leading-order perturbation variables represent the neutral deflection of the basic-state flow to accommodate the harmonic deflection of the interface. In the following subsections, we shall discuss the nature of the functions Ω_1 and Ω_2 for the cylindrical interface.

4.1. *Discussion of* Ω_1

The structure of the mathematical problem is such that the function Ω_1, given by (3.14), does not depend on σ: it is a function only of s_0, q and n. Of more interest than Ω_1 itself are the two associated phase speeds U_θ and U_z, given by (3.15). Isolines of these speeds are plotted in figures 2 and 3. Figures 2(*a*)–2(*c*) present a sequence of isoline plots of

https://doi.org/10.1017/S0022112097007374 Published online by Cambridge University Press

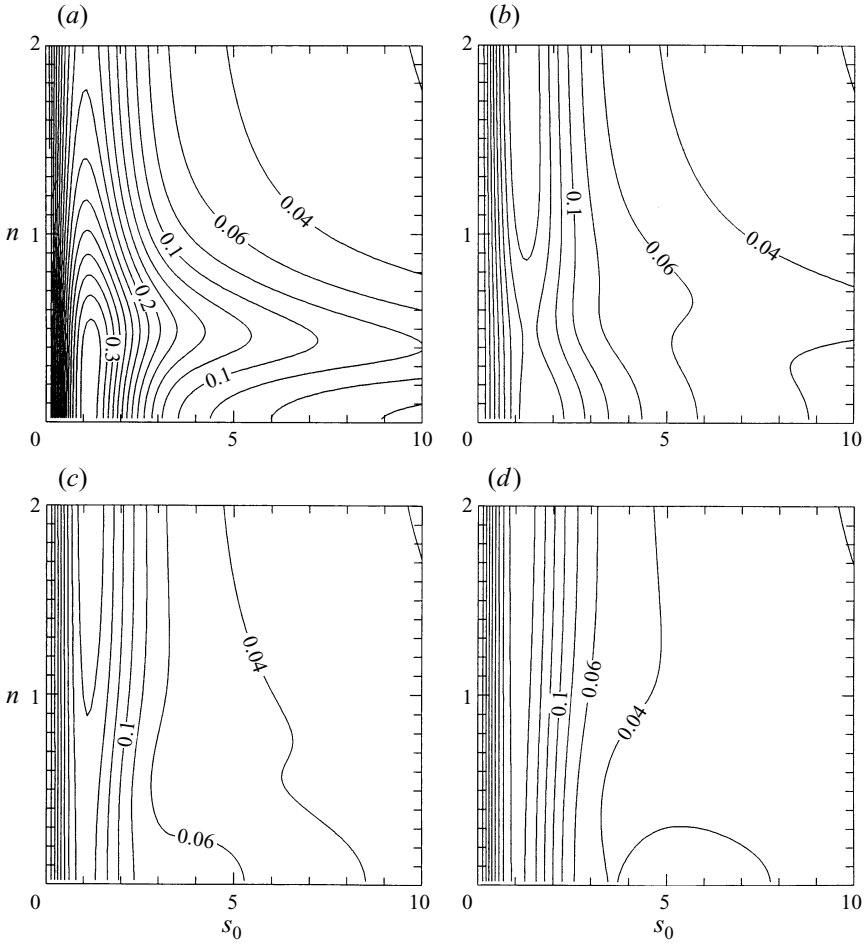


FIGURE 3. Isoline plots of the vertical phase speed, U_z, on the (s_0, n)-plane for (*a*) $q = 0$, (*b*) 1, (*c*) 2 and (*d*) 3. The contour interval is 0.02.

U_θ on the (s_0, n)-plane for $q = 1$, 2 and 3. Note that the zonal phase speed is not defined for the axisymmetric case $q = 0$. From these plots we see that the zonal phase speed is approximately linear in n, decreases for increasing q, is zero for $s_0 = 0$, is largest for s_0 near 1 and asymptotes to a finite value with increasing values of s_0. The case of the single plane interface studied in Part 1 is obtained by taking the double limit of $q \to \infty$ and $s_0 \to \infty$ with their ratio being of unit order; in this limit, $U_\theta \to 0$. Similarly, figures 3(*a*)–3(*d*) present a sequence of isoline plots of U_z on the (s_0, n)-plane for $q = 0$, 1, 2 and 3. From these plots we see that the vertical phase speed is approximately independent of n, decreases moderately for increasing q, is zero for $s_0 = 0$, is largest for s_0 near 1 and decreases in magnitude with increasing values of s_0.

4.2. *Discussion of* Ω_2

The perturbation growth rate, Ω_2, given as an integral in (3.16), is a function of s_0, σ, q and n. It has been verified by asymptotic analysis that in the limit $s_0 \to \infty$ this expression becomes equal to that found in Part 1. As in Parts 1 and 2, Ω_2 is a linear function of σ, although we have not taken advantage of this property in the calculations or discussions. We are primarily interested in the largest growth rate for

https://doi.org/10.1017/S0022112097007374 Published online by Cambridge University Press

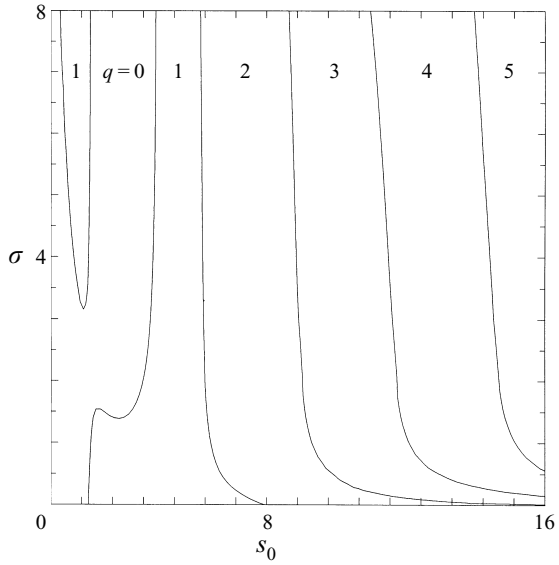


FIGURE 4. The q-regime diagram, showing the regions on the (s_0, σ)-plane for which a specified value of q yields the fastest growing mode.

specified values of s_0 and σ, obtained by maximizing the expression in (3.16) over all possible values of q and n. The values of q and n which achieve the maximum will be referred to as the 'preferred mode'. The principal result of this exercise is a regime diagram given in figure 4, which shows the zonal wavenumber of the preferred mode on the (s_0, σ)-plane for values of s_0 up to 16 and σ up to 8. A region of this plane for which a particular value of q yields the largest growth rate will be referred to as a 'q-regime'; the locations of these regimes are indicated on figure 4. This diagram reveals that the preferred zonal wavenumber increases approximately linearly with increasing s_0. This is expected since, as noted in §2, $q \sim ms_0$ for s_0 large, with $m\,(= m_{max})$ given as a function of σ in figure 1:12. The change in s_0 associated with a unit increase in q is given by

$$\Delta s_0 = \frac{1}{m_{max}(\sigma)}. \tag{4.2}$$

Since m_{max} is an increasing function of σ, the interval Δs_0 is a decreasing function of σ. This is manifest in the increasing tilt with increasing values of s_0 for moderate and large values of σ of the lines bounding q regimes in figure 4.

Since m_{max} goes smoothly to zero for a finite value of $\sigma\,(\approx 0.065)$ in figure 1:12, it follows that the interval Δs_0 goes to infinity as this value of σ is approached from above in figure 4. This is manifest in the lines bounding different q-regimes asymptoting to the line $\sigma = 0.065$ in figure 4. The pattern of q-regimes seen for moderate and large s_0 is broken for small s_0, where a 'hanging $q = 1$ mode' occurs. It is a difficult question whether this is the result of a novel $q = 1$ mode dominant at large σ intruding into the $q = 0$ regime or else an expansion of the $q = 0$ region dominant for small σ into the $q = 1$ regime, dividing it in two. Perhaps some light can be shed on this question by comparing the regime diagram for the cylindrical plume given in figure 4 to that for the Cartesian plume given in figure 2:11. In order to make this comparison, the four categories of modes identified for the Cartesian plume must be related to those possible for the cylindrical plume. In Part 2, a vertical mode is one for which the zonal

https://doi.org/10.1017/S0022112097007374 Published online by Cambridge University Press

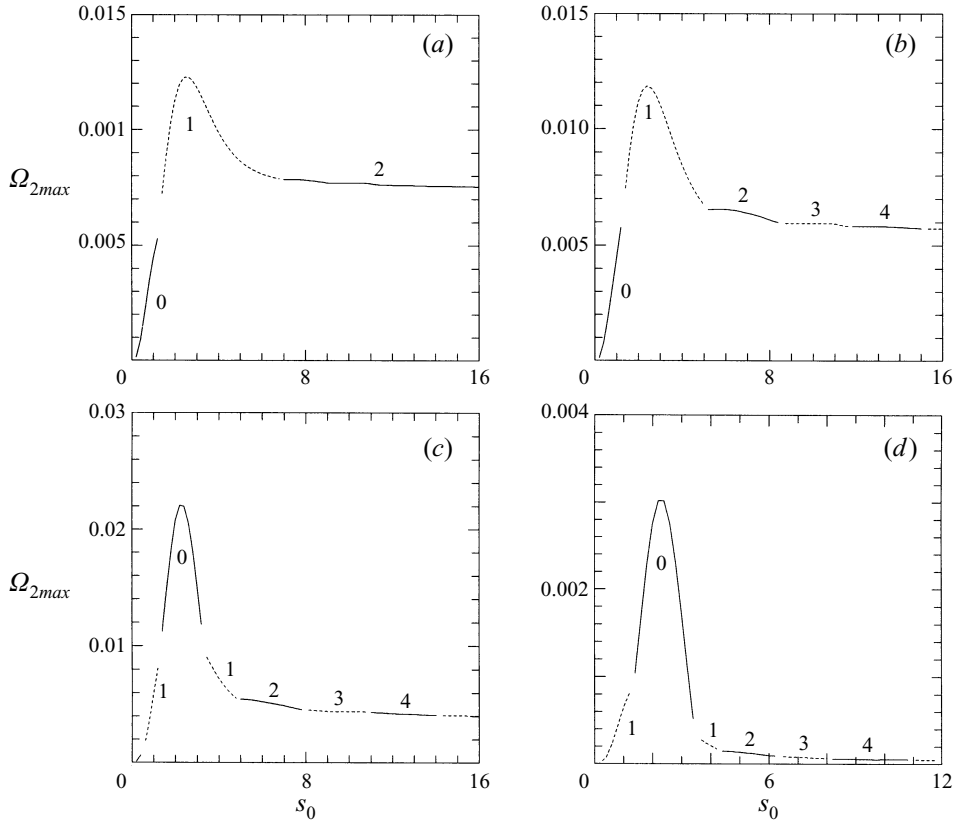


FIGURE 5. Plots of the maximized growth rate Ω_{2max} versus s_0 for representative values of σ: (*a*) 0, (*b*) 1, (*c*) 5 and (*d*) ∞. Note that Ω_{2max}/σ is plotted in (*d*). The numbers next to the curve segments refer to the values of q which yield the maximum, with solid-line segments associated with even values of q and dotted-line segments associated with odd. Note that the maximum growth rate occurs for s_0 between 2 and 3 and for $q = 0$ or 1 for all values of σ.

Cartesian mode	Cylindrical mode
Varicose vertical	$q = 0$
Varicose oblique	q even
Sinuous vertical	Not possible
Sinuous oblique	q odd

TABLE 1. Translation of modes from Cartesian to cylindrical

wavenumber is zero. This obviously translates to the mode $q = 0$. By the same token, oblique modes translate into those having $q > 0$. We shall associate the varicose (sinuous) modes of the Cartesian plume with the cylindrical-plume modes having opposite (same) values of interface deflection at opposite ends of a diameter. This interpretation means that all modes having q even are varicose and those having q odd are sinuous. This interpretation is most clearly evident for the modes $q = 0$ and $q = 1$. This translation is summarized in table 1. Note that the interfaces are sufficiently decoupled in the Cartesian case to permit the existence of the sinuous vertical mode, but this is not possible in the cylindrical case due to the zonal coupling of the interfaces on opposite ends of a diameter.

https://doi.org/10.1017/S0022112097007374 Published online by Cambridge University Press

With table 1, we are in a position to compare figure 4 here with figure 2:11. First, we see that the varicose vertical (Vv) mode, which is dominant for small values of s_0 and σ in the Cartesian case is equivalent to the $q = 0$ regime seen at small values of s_0 and σ in figure 4. Next, the sinuous oblique (So) mode seen at small values of s_0 and moderate values of σ in figure 2:11 has a counterpart in the hanging $q = 1$ mode of figure 4. The sinuous vertical (Sv) mode of figure 2:11 cannot exist for the cylindrical plume. In figure 4, the comparable region is occupied, at least for moderate and large values of σ, by the $q = 0$ mode, which is equivalent to a Vv Cartesian mode. In the Cartesian case, there are only two types of oblique modes, varicose and sinuous, due to the weak coupling between the two interfaces. In the cylindrical case, there is an infinite sequence of oblique modes identified by the value of q. This gives figure 4 a distinctly different appearance for moderate and large values of s_0 from that of figure 2:11. However, the generic similarity between the two is evident: the modes are oblique and the distinction is only in the zonal phase.

It is of some interest to quantify the values of Ω_2 obtained by the maximization process which led to the regime diagram of figure 4. This is done in figure 5, which plots the maximized growth rate, Ω_{2max}, versus s_0 for selected values of σ: 0, 1, 5 and ∞ in parts (*a*), (*b*), (*c*) and (*d*), respectively. Note that in part (*d*) the variable displayed is Ω_{2max}/σ. In these plots, even values of q are indicated by solid lines and odd values by dotted lines, with the associated values of q indicated by the adjacent numbers. Except for the case $\sigma = 0$ seen in part (*a*), the preferred value of q increases with increasing s_0. In the case $\sigma = 0$, the preferred value does not exceed 2, and as s_0 becomes large the preferred value reverts to 0, in agreement with the results in Part 1. In each of the four cases shown in figure 5 the growth rate is zero for $s_0 = 0$, peaks sharply for s_0 slightly larger than 2 and asymptotes to a constant value for large s_0. These asymptotic values agree with those shown in figure 1:12. Note that the strength of the instability is largest for values of cylinder radius close to the value which maximizes the buoyancy flux; see figure 1:7. Note also that the most rapidly growing modes have a preferred zonal wavenumber of either 0 or 1, suggesting that these modes behave anomalously.

The special character of the axisymmetric and helical modes are seen more clearly in figure 6(*a*), which is a repetition of figure 5(*b*), but with all the modal lines shown, not merely the largest. From this we see (i) that the maximum growth rate of modes varies inversely with the zonal wavenumber except for the helical mode, (ii) that modes with $q = 0$ and 1 have growth rates significantly larger than those having $q \geqslant 2$ and (iii) the growth rate of the helical mode is anomalously large. Figure 6(*b*) shows a comparable variation of growth rate with plume size for the sinuous mode of the Cartesian plume for various values of the transverse wavenumber; the varicose mode exhibits similar behaviour. In this case, no anomalous variation is seen, indicating that the geometry of the plume (two-dimensional vs. cylindrical) plays an important role in the nature of the instability.

It is seen from figure 5 that the fastest growing mode has a zonal wavenumber $q = 1$ for small values of the Prandtl number, σ, and $q = 0$ for moderate values of σ. The appropriate value of σ for the ammonium-chloride experiment is not clear, as the Prandtl number of water varies by at least a factor of 2 for the temperature range of that experiment (see Appendix 1 of Batchelor 1967). Wettlauffer *et al.* (1996) observed plume instability with $q = 0$ during the freezing of sea ice. Since the Prandtl number of cold water (in the sea-ice experiment) is higher than that of warm water (in the ammonium-chloride experiment) and our theory predicts q for the fastest growing mode to decrease with increasing σ, the differing character of instability observed in the two experiments is compatible with the results of the present theory. This discussion

https://doi.org/10.1017/S0022112097007374 Published online by Cambridge University Press

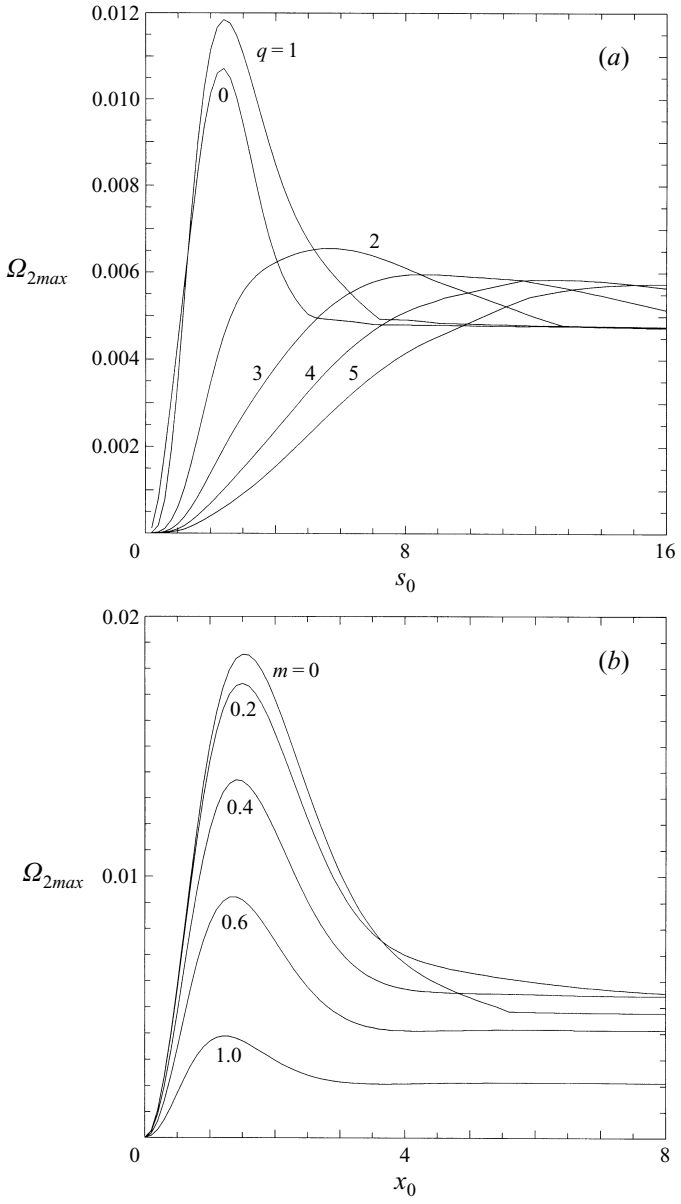


FIGURE 6. Comparison of the maximized growth rate Ω_{2max} versus s_0 for $\sigma = 1$ in the case of (*a*) a cylindrical plume and (*b*) a Cartesian plume with varicose instability. Note the anomalously large growth rate of the $q = 1$ mode in the cylindrical case. The kinks appearing in some of the curves are real; there is a jump in the preferred vertical wavenumber at the kinks.

highlights the need for an improved theory of plume instability which takes into account the variability of Prandtl number with temperature.

The vertical wavenumber, n_{max}, associated with the maximized growth rate is plotted versus s_0 for selected values of σ: 0, 1, 5 and ∞ in figures 7(*a*)–7(*d*). These plots are discontinuous since the value of n changes depending on the value of q. The numbers adjacent to the segments of curves give the preferred value of q associated with each segment. The values of n_{max} are all of unit order, but there is no clear pattern in the

https://doi.org/10.1017/S0022112097007374 Published online by Cambridge University Press

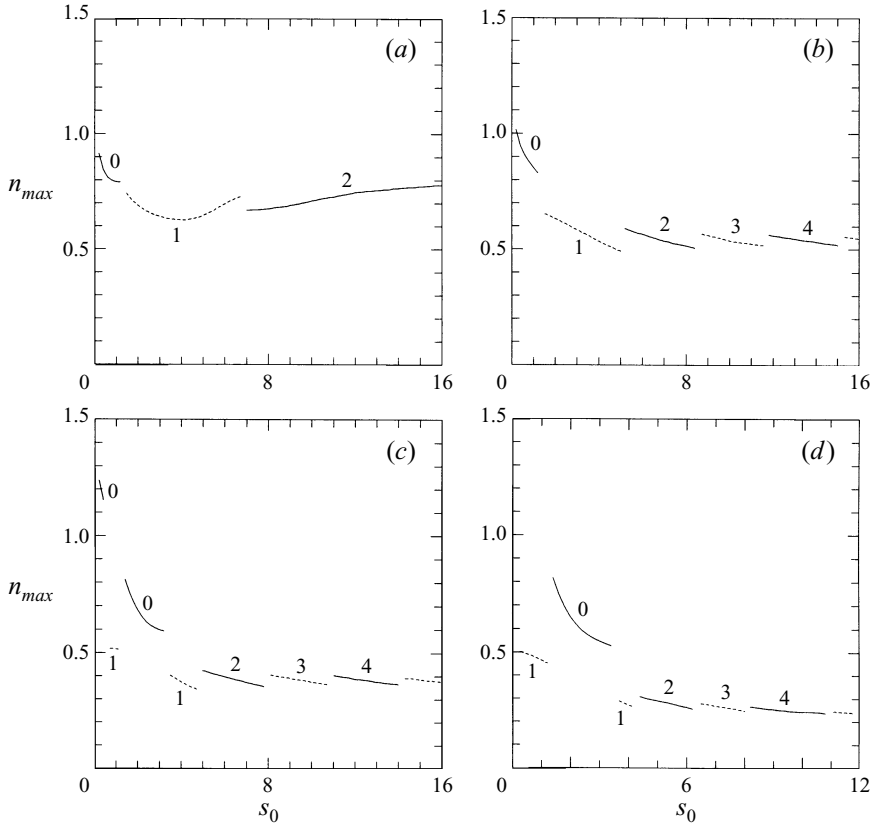


FIGURE 7. Plots of the optimal vertical wavenumber n_{max} versus s_0 for representative values of σ: (*a*) 0, (*b*) 1, (*c*) 5 and (*d*) ∞. The numbers next to the curve segments refer to the value of q which yields the maximum.

trend either as a function of s_0 or σ, excepting that the values for $q = 0$ are consistently larger than for $q = 1$. The asymptotic values n_{max} in the limit of $s_0 \to \infty$ as a function of σ approach the function shown in figure 1:12.

5. Summary and concluding remarks

5.1. *Summary*

The linear stability of a circular interface, enclosing compositionally buoyant material in a thermally stably stratified fluid, has been investigated. Material diffusivity is neglected, so that the interface remains sharp and identifiable. A density jump is assumed to accompany the jump in composition and this acts to drive vertical motion parallel to the unperturbed interface. This motion advects the heat vertically, causing a local change in temperature which is balanced by radial diffusion of heat in the unperturbed state. We have investigated the stability of this basic state as the circular interface experiences small-amplitude harmonic distortion characterized by a zonal wavenumber q (restricted to integer values) and vertical wavenumber n.

The strength of the density jump driving the flow and instability is characterized by the Reynolds number, $R = UL/\nu$ where L and U are the units of length and velocity associated with salt fingers: $L = (\nu\kappa/\alpha\gamma)^{1/4}$ and $U = \beta\tilde{C}(g\kappa/\alpha\gamma\nu)^{1/2}$. Since the basic

https://doi.org/10.1017/S0022112097007374 Published online by Cambridge University Press

state is baroclinic, there is no minimum critical Reynolds number. The stability analysis has been performed assuming that $R \ll 1$, with the dependent variables and the growth rate being expanded in powers of R. As in the cases of the single flat interface and two parallel interfaces studies in Parts 1 and 2, the dominant-order term (of order R) in the expansion of the growth rate is imaginary, indicating an oscillation, and stability of the interface is determined by the second term (of order R^2) in the expansion. In the Cartesian analyses of Part 1 and Part 2 the growth rate to order R^2 was evaluated by a straightforward (though complicated) analytic solution of the perturbation problem at dominant and next order in powers of R. This procedure fails for the cylindrical plume, and an alternative procedure has been developed in which the growth rate is expressed as an integral involving only the basic-state and dominant-order perturbation variables.

It is found that basic state and the interface shape are unstable for some wavenumber for all values of Prandtl number, σ, and interface radius, s_0. The preferred zonal wavenumber grows roughly linearly with s_0 except for small values of σ: $\sigma < 0.065$. The preferred vertical wavenumber remains of unit order for all values of s_0 and σ. The growth rate is largest for s_0 slightly larger than 2 and for modes having zonal wavenumbers $q = 0$ or 1.

The instability has the appearance of an overstable oscillation. The dimensional phase speeds in the zonal and vertical directions are of order U, with an associated period of oscillation of order

$$\tau_{osc} = \frac{L}{U} = \frac{\nu}{U^2} = \frac{\nu\rho}{(\Delta\rho)_c g L}, \tag{5.1}$$

while the time scale of growth is

$$\tau_{grow} = \frac{L}{UR} = \frac{\nu}{U^2} = \left[\frac{\nu\rho}{(\Delta\rho)_c}\right]^2 \frac{\alpha}{\kappa g}\left(\frac{\mathrm{d}T}{\mathrm{d}z}\right). \tag{5.2}$$

Here $(\Delta\rho)_c$ is the jump in density associated with the prescribed jump in composition.

5.2. *Comments on the physical cause of the instability*

As noted previously, the most unstable mode of a cylindrical interface is helical (having zonal wavenumber 1) for small Prandtl number and axisymmetric ($q = 0$) for large. We shall attempt to explain this behaviour physically in this subsection. The explanation will be based on the assumption that a plume of compositionally buoyant material seeks to be as vigorous as possible, with vigour being quantified by buoyancy flux (see §1:3.4).

Vertical motion of fluid within the interface is driven by its compositional buoyancy and retarded by both thermal buoyancy and viscous drag. The vigour of this motion can be increased by increasing the rate of heat transfer across the interface and by decreasing the amount of viscous drag. In the limit of small Prandtl number, thermal diffusion occurs readily and the limiting factor is the viscous drag, while in the limit of large Prandtl number, thermal diffusion is weak and hence is the limiting factor. These two limits may be seen mathematically in the perturbation equations (A 1)–(A 11) of the Appendix; in the limit $\sigma \ll 1$, the forcing is dominantly mechanical while if $1 \ll \sigma$, it is dominantly thermal. (Given the above argument, the reader might wonder why a solution to the problem can exist at all in the limit of $\sigma \to \infty$, since thermal diffusion becomes arbitrarily small in that limit. The answer is that the physical length and velocity scales are dependent on the magnitude of the thermal diffusivity (see (2.6)) and these indeed become small in this limit.)

https://doi.org/10.1017/S0022112097007374 Published online by Cambridge University Press

It may be seen from the basic-state solution (2.10)–(2.11) that viscous drag on the fluid contained by the interface is caused by the surrounding collar of fluid which moves in the opposite direction. This drag is diminished if the counterflowing fluids are in less immediate contact. This diminution is accomplished by the helical instability, having $q = 1$, which shifts the counterflow to one side of the interface. (The upward flow in the plume and the downward counterflow in fully developed helical flow may be visualized as the strands of a two-stranded rope.) This mode of instability is to be preferred when viscosity is the limiting factor: when the Prandtl number is small. Note that this mode of instability appears to have no counterpart in the case of planar interfaces studied in Parts 1 and 2.

Plume vigour is increased by increasing the diffusion of heat across the interface, which may be accomplished by increasing the surface area of the interface. This increase is accomplished most readily by the axisymmetric instability, having $q = 0$, coupled with a large vertical wavenumber. This mode should be preferred when thermal diffusion is the limiting factor: when the Prandtl number is large. It may be seen from figure 7 that the vertical wavenumber for $q = 0$ is systematically larger than that for $q = 1$, lending support to the present heuristic argument.

These arguments assume that the radius of the cylindrical interface is close to the value which maximizes buoyancy flux. If the radius is significantly larger, the preferred mode has a wavenumber greater than unity, as seen in figure 4. If $q \neq 1$, the instability appears ineffective in reducing its viscous drag, and enhancement of the vigour of the plume is likely accomplished by increasing thermal diffusion.

5.3. *Some limitations of the present model*

As noted in §4.2, the present model, with its assumption of constant Prandtl number, may not be accurate for an aqueous solution if the temperature variations experienced are large, of order several tens of degrees centigrade. The principal cause of the variation of Prandtl number is the variation of the dynamic viscosity with temperature. An improved model should take this variation into account.

One motivation of the present study is the desire to understand better the nature of the small-scale compositionally driven flow which may occur within Earth's core in association with the operation of the geodynamo. An obvious shortcoming of the present analysis is that it ignores the effects of rotation and magnetic fields which are virtually certain to be of dynamical importance in the core. However, it is anticipated that the novel procedure developed in the Appendix, in which the growth rate is determined in terms of the basic-state and leading-order perturbation variables, may be generalized and used to solve the problem of stability of a cylindrical plume in the presence of rotation and/or magnetic fields. Efforts are underway to solve these problems.

Another shortcoming of the present study, as well as those in Part 1 and Part 2, is that the composition in the plume is uniform with a sharp discontinuity at an interface. A more realistic situation is that in which the composition varies continuously with radius. It may be possible to represent the solution of that more realistic problem as a convolution involving the solution presented in this paper.

This work was supported in part by grants INT-9412211 and EAR-9417481 from the National Science Foundation. This is publication 387 of the Geophysical Fluid Dynamics Institute, Florida State University, Tallahassee, Florida.

https://doi.org/10.1017/S0022112097007374 Published online by Cambridge University Press

Appendix. Determination of the solvability condition

In this Appendix, a solvability condition for the first-order stability problem is found. The relevant equations, governing the first-order variables, are

$$s^2\,\mathrm{L}(u_1)-u_1-2qv_1 = s^2F_u, \tag{A 1}$$

$$s^2\,\mathrm{L}(v_1)-v_1-2qu_1 = s^2F_v, \tag{A 2}$$

$$\mathrm{L}(p_1)-T_1 = F_p, \tag{A 3}$$

$$\mathrm{L}(w_1)+T_1+n^2p_1 = F_w \tag{A 4}$$

and

$$\mathrm{L}(T_1)-w_1 = F_T, \tag{A 5}$$

where

$$F_u(s) = n(\mathrm{d}p_1/\mathrm{d}s)+\bar{\Omega}_1(s)\,u_0(s), \tag{A 6}$$

$$F_v(s) = -(qn/s)\,p_1(s)+\bar{\Omega}_1(s)\,v_0(s), \tag{A 7}$$

$$F_p(s) = -2\mathrm{i}(\mathrm{d}\bar{w}/\mathrm{d}s)\,u_0(s), \tag{A 8}$$

$$F_w(s) = \mathrm{i}(\mathrm{d}\bar{w}/\mathrm{d}s)\,u_0(s)+\bar{\Omega}_1(s)\,w_0(s), \tag{A 9}$$

$$F_T(s) = \mathrm{i}\sigma(\mathrm{d}\bar{T}/\mathrm{d}s)\,u_0(s)+\sigma\bar{\Omega}_1(s)\,T_0(s) \tag{A 10}$$

and

$$\bar{\Omega}_1(s) = \Omega_1+\mathrm{i}n\bar{w}(s). \tag{A 11}$$

These equations are subject to conditions (2.32), (2.33), (2.37), with subscripts 1 where appropriate, and homogeneous versions of (2.34) and (2.35):

$$\text{at } s = s_0 \qquad \mathrm{d}p_1/\mathrm{d}s \quad \text{and} \quad \mathrm{d}T_1/\mathrm{d}s \quad \text{are continuous.} \tag{A 12}$$

Also, condition (2.36) requires that

$$\Omega_2 = \mathrm{i}u_1(s_0). \tag{A 13}$$

We wish to exploit condition (A 13) to obtain an expression for Ω_2 in terms of the leading-order and basic-state variables. We begin by considering the horizontal momentum equations (A 1) and (A 2), which form a coupled set for u_1 and v_1 in terms of p_1, Ω_1, u_0, v_0 and $\bar{w}$. This set may be uncoupled by adding and subtracting them. Dividing the result by s^2 yields

$$\left[\mathrm{L}-\frac{(1\pm 2q)}{s^2}\right](u_1\pm v_1) = F_u\pm F_v, \tag{A 14}$$

where the operator L is defined by (2.30). The equation with the upper sign has homogeneous modes $I_{q+1}(ns)$, $K_{q+1}(ns)$, while that with the lower sign has homogeneous modes $I_{q-1}(ns)$, $K_{q-1}(ns)$. In order to extract the value of u_1 at $s = s_0$ in terms of integrals of the forcing functions, we shall multiply (A 14) by $sG_\pm$ and integrate from $s = 0$ to $s = \infty$, i.e.

$$\int_0^\infty \left\{\left[\mathrm{L}-\frac{(1\pm 2q)}{s^2}\right](u_1\pm v_1)\right\} G_\pm(s;s_0)\,s\,\mathrm{d}s = \int_0^\infty [F_u(s)\pm F_v(s)]\,G_\pm(s;s_0)\,s\,\mathrm{d}s, \tag{A 15}$$

where

$$G_\pm(s;s_0) = -s_0\begin{cases} K_{q\pm1}(ns_0)\,I_{q\pm1}(ns) & \text{for} \quad 0<s<s_0 \\ I_{q\pm1}(ns_0)\,K_{q\pm1}(ns) & \text{for} \quad s_0<s. \end{cases} \tag{A 16}$$

Note that $G_\pm$ is a Greens' function; it satisfies the following jump conditions:

$$\langle G_\pm\rangle = 0 \quad \text{and} \quad \langle \mathrm{d}G_\pm/\mathrm{d}s\rangle = 1. \tag{A 17}$$

https://doi.org/10.1017/S0022112097007374 Published online by Cambridge University Press

We may integrate the left-hand side integral of (A 15) by parts. Using continuity conditions (A 12) and noting that $G_\pm$ satisfies the homogeneous operator, we have

$$u_1(s_0) \pm v_1(s_0) = \int_0^\infty [F_u(s) \pm F_v(s)]\, G_\pm(s; s_0) \frac{s}{s_0} \mathrm{d}s. \tag{A 18}$$

We have made use of (A 17) in writing (A 18). Adding the two versions of (A 18) and using (A 13), we obtain

$$\mathrm{i}u_1 = \Omega_2 = \frac{\mathrm{i}}{2} \int_0^\infty [(F_u + F_v)\, G_+ + (F_u - F_v)\, G_-] \frac{s}{s_0} \mathrm{d}s. \tag{A 19}$$

Combining (3.8), (3.9), (A 6) and (A 7) we have that

$$F_u \pm F_v = n s^{\pm q} \left[\frac{\mathrm{d}}{\mathrm{d}s} (s^{\mp q} p_1) + \bar{\Omega}_1 \frac{\mathrm{d}}{\mathrm{d}s} (s^{\mp q} V) \right], \tag{A 20}$$

where

$$V = s_0 \sum_{j=1}^{3} B_j R_j \tag{A 21}$$

and B_j and R_j are given in (3.10) and (3.11). Note that V is closely related to v_0: compare (A 21) with (3.9).

Substituting (A 20) into (A 19) and integrating by parts, we have

$$\Omega_2 = -\mathrm{i}n \int_0^\infty p_1 H_n \frac{s}{s_0} \mathrm{d}s - n \int_0^\infty \left[\mathrm{i}\bar{\Omega}_1 H_n - \frac{n}{2} \frac{\mathrm{d}\bar{w}}{\mathrm{d}s} (G_+ + G_-) \right] V \frac{s}{s_0} \mathrm{d}s, \tag{A 22}$$

where

$$H_n(s; s_0) = \frac{1}{2s} \left[s^{-q} \frac{\mathrm{d}(s^{1+q} G_+)}{\mathrm{d}s} + s^q \frac{\mathrm{d}(s^{1-q} G_-)}{\mathrm{d}s} \right] = n s_0 \begin{cases} K_q'(n s_0)\, I_q(n s) \\ I_q'(n s_0)\, K_q(n s). \end{cases} \tag{A 23}$$

Note that H_n satisfies the following jump conditions:

$$\langle H_n \rangle = 1 \quad \text{and} \quad \langle \mathrm{d}H_n/\mathrm{d}s \rangle = 0. \tag{A 24}$$

To make further progress, we must be able to write the integral of $p_1 H_n$ appearing in (A 22) in terms of leading-order and basic-state variables. We begin this procedure by forming L^2(A 4) + (A 4) + (A 3) + L(A 5), which yields a sixth-order non-homogeneous ordinary differential equation for p_1:

$$\mathrm{L}^3(p_1) + \mathrm{L}(p_1) + n^2 p_1 = F_{tot}, \tag{A 25}$$

where

$$F_{tot} = \mathrm{L}^2(F_p) + F_p + F_w + \mathrm{L}(F_T). \tag{A 26}$$

Note that the homogeneous modes for (A 25) are $I_q(\xi_j s)$ and $K_q(\xi_j s)$ where ξ_j is defined by (3.12).

Next, consider the expression

$$Q = Q_n - \sum_{j=1}^{3} \frac{n^2 Q_j}{3n^2 + 2\mu_j}, \tag{A 27}$$

where

$$\{Q_n, Q_j\} = \int_0^\infty F_{tot}(s) \{H_n(s; s_0), H_j(s; s_0)\} \frac{s}{s_0} \mathrm{d}s \tag{A 28}$$

and the functions H_j are given by (3.22). Note that H_j obey the jump conditions (A 24).

https://doi.org/10.1017/S0022112097007374 Published online by Cambridge University Press

It is clear from (A 8)–(A 10) and (A 26)–(A 28) that Q is known in terms of zeroth-order variables. It remains to show that the integral involving p_1 which appears in (A 22) can be expressed in terms of Q. To begin this process, substitute for F_{tot} in (A 28) using (A 26) and integrate by parts. The results may be expressed as

$$Q_n = n^2 \int_0^\infty p_1(s)\, H_n(s;s_0)\frac{s}{s_0}\,\mathrm{d}s + \mathrm{J}_n(N_n) \tag{A 29}$$

and

$$Q_j = \mathrm{J}_j(N_j) \tag{A 30}$$

where

$$\mathrm{J}_\gamma(f) = \frac{\mathrm{d}H_\gamma}{\mathrm{d}s}(s_0)\langle f\rangle - H_\gamma(s_0+)\left\langle\frac{\mathrm{d}f}{\mathrm{d}s}\right\rangle - \frac{\mathrm{d}f}{\mathrm{d}s}(s_0-) \tag{A 31}$$

for $\gamma = n,j$,

$$N_n = \mathrm{L}^2(p_1) + p_1 \tag{A 32}$$

and

$$N_j = \mathrm{L}^2(p_1) + \mu_j\,\mathrm{L}(p_1) + (1+\mu_j^2)\,p_1. \tag{A 33}$$

Note that the jump factor (A 31) reduces to

$$\mathrm{J}_\gamma(f) = -\frac{\mathrm{d}f}{\mathrm{d}s}(s_0) \tag{A 34}$$

if the function f and its first derivative are continuous at $s = s_0$, as is the case, for example, for any first-order variable.

The integrals disappear from (A 30) by virtue of (3.13), leaving only the desired integral in (A 29). At this point the solution scheme appears to be in trouble due to the occurrence of the first-order variable p_1 in the jump terms. However, these terms can be shown to be identically zero, as follows. Using (A 3) and (A 5), the N simplify to

$$N_n = F_n + p_1 + w_1 \tag{A 35}$$

and

$$N_j = F_j + (1+\mu_j^2)\,p_1 + w_1 + \mu_j\,T_1, \tag{A 36}$$

where

$$F_n = \mathrm{L}(F_p) + F_T \tag{A 37}$$

and

$$F_j = \mathrm{L}(F_p) + \mu_j F_p + F_T. \tag{A 38}$$

Now (A 27), (A 29), (A 30), (A 35) and (A 36) may be combined to yield

$$\begin{aligned} Q = n^2 \int_0^\infty p_1 H_n \frac{s}{s_0}\,\mathrm{d}s + \mathrm{J}_n(F_n) - \sum_{j=1}^{3}\frac{n^2\,\mathrm{J}_j(F_j)}{3n^2+2\mu_j} + \left[\sum_{j=1}^{3}\frac{n^2\mu_j}{3n^2+2\mu_j}\right]\frac{\mathrm{d}T_1}{\mathrm{d}s}(s_0) \\ + \left[\sum_{j=1}^{3}\frac{n^2}{3n^2+2\mu_j} - 1\right]\frac{\mathrm{d}w_1}{\mathrm{d}s}(s_0) + \left[\sum_{j=1}^{3}\frac{n^2(1+\mu_j^2)}{3n^2+2\mu_j} - 1\right]\frac{\mathrm{d}p_1}{\mathrm{d}s}(s_0). \end{aligned} \tag{A 39}$$

By virtue of (1:B 29) the coefficients of all first-order terms in (A 39) disappear. Combining the simplified (A 39) with (A 22), we have

$$\Omega_2 = -n\int_0^\infty \left[\mathrm{i}\bar{\Omega}_1 H_n - \frac{n}{2}\frac{\mathrm{d}\bar{w}}{\mathrm{d}s}(G_+ + G_-)\right] V\frac{s}{s_0}\,\mathrm{d}s - \frac{\mathrm{i}}{n}\left[Q - \mathrm{J}_n(F_n) + \sum_{j=1}^{3}\frac{n^2\,\mathrm{J}_j(F_j)}{3n^2+2\mu_j}\right]. \tag{A 40}$$

At this point we have an expression for Ω_2 in terms of leading-order variables, with Q given by (A 27) and (A 28) and F_{tot} given by (A 26). Substituting these expressions

https://doi.org/10.1017/S0022112097007374 Published online by Cambridge University Press

into (A 40) and integrating by parts, we have the somewhat simpler expression (i.e. not containing the jump operators) given by (3.16). In writing (3.16) we have made use of (A 11), (A 21) and (3.11), plus

$$G_+ + G_- = \frac{2}{n^2}\left(\frac{q^2 R_n}{s} - \frac{\mathrm{d}H_n}{\mathrm{d}s}\right), \tag{A 41}$$

which may be verified using standard formulas.

REFERENCES

Abramowitz, M. & Stegun, I. A. 1970 *Handbook of Mathematical Functions*. US National Bureau of Standards.

Batchelor, G. K. 1967 *An Introduction to Fluid Dynamics*. Cambridge University Press.

Chen, C. F. 1995 Experimental study of convection in a mushy layer during directional solidification. *J. Fluid Mech.* **293**, 81–98.

Chen, C. F. & Chen, F. 1991 Experimental study of directional solidification of aqueous ammonium chloride solution. *J. Fluid Mech.* **227**, 567–586.

Copley, S. M., Giamei, A. F., Johnson, S. M. & Hornbecker, M. F. 1970 The origin of freckles in unidirectionally solidified castings. *Metall. Trans.* **1**, 2193–2204.

Drazin, P. G. & Reid, W. H. 1981 *Hydrodynamic Stability*. Cambridge University Press.

Eltayeb, I. A. & Loper, D. E. 1991 On the stability of vertically oriented double-diffusive interfaces. Part 1. A single plane interface. *J. Fluid Mech.* **228**, 149–181.

Eltayeb, I. A. & Loper, D. E. 1994 On the stability of vertically oriented double-diffusive interfaces. Part 2. Two parallel interfaces. *J. Fluid Mech.* **267**, 251–273.

Hellawell, A., Sarazin, J. R. & Steube, R. S. 1993 Channel convection in partly solidified systems. *Phil. Trans. R. Soc. Lond.* A **345**, 507–544.

Howard, L. N. & Veronis, G. 1987 The salt-finger zone. *J. Fluid Mech.* **183**, 1–23.

Howard, L. N. & Veronis, G. 1992 Stability of salt fingers with negligible diffusivity. *J. Fluid Mech.* **239**, 511–522.

Jaupart, C. & Tait, S. R. 1995 Dynamics of differentiation in magma reservoirs. *J. Geophys. Res.* **100**, 17615–17636.

Loper, D. E. & Moffatt, H. K. 1993 Small scale hydromagnetic flow in the Earth's core: rise of a vertical buoyant plume. *Geophys. Astrophys. Fluid Dyn.* **68**, 177–202.

Moffatt, H. K. & Loper, D. E. 1994 The magnetostrophic rise of a buoyant parcel in the Earth's core. *Geophys. J. Intl* **117**, 394–402.

Wettlauffer, J. S., Worster, M. G. & Huppert, H. E. 1997 Natural convection during solidification of an alloy from above with application to the evolution of sea ice. *J. Fluid Mech.* **244**, 291–316.

Worster, M. G. 1997 Convection in mushy layers. *Ann. Rev. Fluid Mech.* **29**, 91–122.

https://doi.org/10.1017/S0022112097007374 Published online by Cambridge University Press